Electrochimica Acta 254 (2017) 201–213

Contents lists available at ScienceDirect

Electrochimica Acta

journal homepage: www.elsevier.com/locate/electacta

# Tailoring electroactive surfaces by non-template molecular assembly. Towards electrooxidation of L-cysteine

Mireya Santander-Nelli[a,b,*], Carlos P. Silva[a,b], Javier Espinoza-Vergara[a,b], Juan F. Silva[a,b], Camila F. Olguín[a,b], Diego Corte's-Arriagada[c], José H. Zagal[a,b], Fernando Mendizabal[d], Ismael Díez-Pérez[e], Jorge Pavez[a,b,*]

[a] Departamento de Química de los Materiales, Facultad de Química y Biología, Universidad de Santiago de Chile, Av. Libertador B. O'Higgins 3363, Casilla 40, Correo 33, Santiago, Chile
[b] Soft Matter Research and Technology Center, SMAT-C, Santiago, Chile
[c] Programa Institucional de Fomento a la Investigación, Desarrollo e Innovación, Universidad Tecnológica Metropolitana, Ignacio Valdivieso 2409, P.O. Box 8940577, San Joaquín, Santiago, Chile
[d] Depto. de Química, Fac. de Ciencias, Universidad de Chile, Casilla 653, Santiago, Chile
[e] Department of Material Science and Physical Chemistry & Institute of Theoretical and Computational Chemistry (IQTC), University of Barcelona, Diagonal 645, and Institute for Bioengineering of Catalonia (IBEC), Baldiri Reixac 15-21, 08028 Barcelona, Catalonia, Spain

ARTICLE INFO

*Article history:*
Received 6 July 2017
Received in revised form 14 September 2017
Accepted 14 September 2017
Available online 18 September 2017

*Keywords:*
SAMs
single walled carbon nanotube
bottom-up construction
molecular assembly
modified electrode
DFT

ABSTRACT

We have prepared a nanoelectrode ensemble containing vertically aligned single walled carbon nanotubes (SWCNTs) using a non-template molecular self-assembling strategy. We used a bottom-up construction approach to assemble amino functionalized SWCNTs (*af*-SWCNTs) in a well-defined architecture. These *af*-SWCNTs were linked and vertically aligned to pre-formed self-assembled monolayers of 4-MBA. A Cobalt(II) tetracarboxyphthalocyanine ($Co(COOH)_4Pc$) complex was covalently bonded to external portion of *af*-SWCNTs to complete the final nanoelectrode ensemble. X-ray photoelectron spectroscopy (XPS) and Atomic Force Microcopy (AFM) confirmed the effectiveness of the assembling steps on the gold surface starting from the Au/MBA SAMs. The system Au/4-MBA/*af*-SWCNTs shows an interface with large ordered array, which exhibits a high activity for the electrooxidation of L-cysteine (L-cys). Theoretical calculations suggest that the incorporation of the *af*-SWCNTs increased the activity of the assembly to electronic transfer and it was observed that the electrooxidation reaction is energetically favorable.



## 1. Introduction

Electroactive surfaces built from molecular assemblies constitute one of the most important frontiers in modern electrochemical science. The possibility to build modified hybrid electrodes combining two (or more) kinds of materials, such as carbon nanotubes (CNTs) and conjugated organic or inorganic molecules, is becoming a very active area in surface science due to the wide range of potential applications, including photovoltaic and optoelectronics devices [1–3], sensors [4–8], in electrocatalysis for oxygen reduction reaction (ORR) in fuel cell [9–14], and for the immobilization of enzymes and nucleic acids in bioelectronics systems [15–17].

The carbon nanotubes (CNTs) are an excellent supporting conductive material, and in some cases it present a synergistic effect causing a decrease of the overpotential in some electrochemical reactions [18–20]. Unfortunately, they are not soluble in common organic solvent [21] and tend to form agglomerates and molecular bundles at surface and interfaces. For this reason it is necessary to create chemical functionalities mostly located at the edges of tubes [22], like carboxylic or amine groups, increasing their solubility. On top of these functionalities, it is possible to create chemical links between the CNTs and redox active molecules of interest and confined them on surfaces [23,24] where the electron transfer (ET) process can be accelerated, as compared to the case where these redox species are simply adsorbed on the CNTs, as demonstrated recently for the reduction of $O_2$ on Fe phthalocyanine axially linked to SWCNTs [25], where axial linking enhances the catalytic activity of FePc as compared to that directly adsorbed on the carbon nanotubes. On the other hand,

* Corresponding authors.
*E-mail addresses:* mireya.santander@usach.cl (M. Santander-Nelli), jorge.pavez@usach.cl (J. Pavez).

http://dx.doi.org/10.1016/j.electacta.2017.09.082
0013-4686/

it is possible to vertically assemble CNTs using different strategies including simple adsorption by profiting the π-π interactions of aromatic rings of molecules anchored on gold, such as thiophenol, 4,4'dithiopyridine, and biphenylthiol, which can produce highly ordered molecular assemblies [26]. The vertical alignment can also be achieved by locating negatively charged carboxylic groups at the edges of the CNTs that can interact with positively charged silver surface [27]. Covalent bonds can also be formed between the functional groups in the CNTs and organic molecules attached to an electrode surface. This strategy has been successful mainly when using CNTs with —*COOH* functional groups, which can form amide bonds with amino groups present on organic molecules confined on the electrode. Using this approach Chou et *al.* [28] modified gold substrates with alkanethiols of different chain lengths, which were further modified with CNTs, resulting in a remarkable increase of the electrochemical reactivity of the surface. They also modified glassy carbon electrodes by electrografting with aromatic amines (phenyldiamine) [29], which show similar properties to those reported by Chou. Silicon and platinum surfaces have also been used for these types of modifications [30–32].

In this work, we describe the molecular assembly of an electrochemically active system composed of single-wall amine-functionalized carbon nanotubes (*af*-SWCNTs) vertically aligned on self-assembled monolayers of aromatic thiol (4-mercaptobenzoic acid, 4-MBA) on an Au (111) substrate. The SWCNTs were linked to the SAMs by coupling using carbodiimide by formation of an amide bond between the amine group in 4-ATP and *af*-SWCNTs, and the carboxylic group of 4-MBA.

On the other hand, MN4 metal macrocyclic complexes are very versatile molecules that present electrocatalytic activity for a myriad of oxidation and reduction reactions [33–54]. In particular, when confined on graphite or carbon surfaces, they catalyze the oxidation of thiols (RSH) to give the corresponding disulfides (RSSR) [42–52]. Of special interest is the oxidation of the aminoacid L-cysteine, which bears a −SH functionality and undergoes oxidation to give the corresponding disulfide Lcystine [48–52].

## 2. Experimental

### 2.1. Materials and reagents

4-aminothiophenol (97%), p-phenylenediamine (99.0%), N-(3-Dimethylaminopropyl)-N′-ethylcarbodiimide hydrochloride (EDAC), 1-hydroxybenzotriazole hydrate (HOBt), were obtained from Sigma-Aldrich; 4-mercaptobenzoic acid (95%) was obtained from Tokyo Chemical Industry Co. Single-Walled Carbon Nanotube (SWCNTs) average diameter 1.1 nm and length 0.45 to 2.3 μm were purchased from South West Nano Technologies and used as provided. Cobalt tetracarboxylic acid phthalocyanine (Co(COOH)$_4$Pc) was synthesized according to a method described in the previous section (see the Supplementary Data section 1). The reagents and solvents were of analytical grade and were used without further treatment.

### 2.2. Instruments

Electrochemical experiments were performed with a Potentiostat/Galvanostat PGSTAT302N Autolab, using a conventional three-electrode electrochemical cell. An Ag/AgCl electrode and Pt wire were employed as reference and counter electrodes respectively and as working electrode was a thin vapor deposited Au film on glass (12 × 12 mm slides purchased from Arrandee, Germany). The tapping mode AFM images were obtained using a Digital Instruments NanoScope IIIa. IR (KBr discs) was recorded on Spectrum 64 PerkinElmer spectrophotometer. The XPS measurements were performed on a PHI 550 Multitechnique System (from Physical Electronics) in a ultra high vacuum chamber pressure.

### 2.3. Electrodes modification

#### 2.3.1. Cutting and amine-functionalization of carbon nanotubes

The commercial SWCNTs were cutting following a reported procedure of acid digestion [55]. The acid treatment of SWCNTs produces carboxylic acid groups on its surface (edges mostly on),

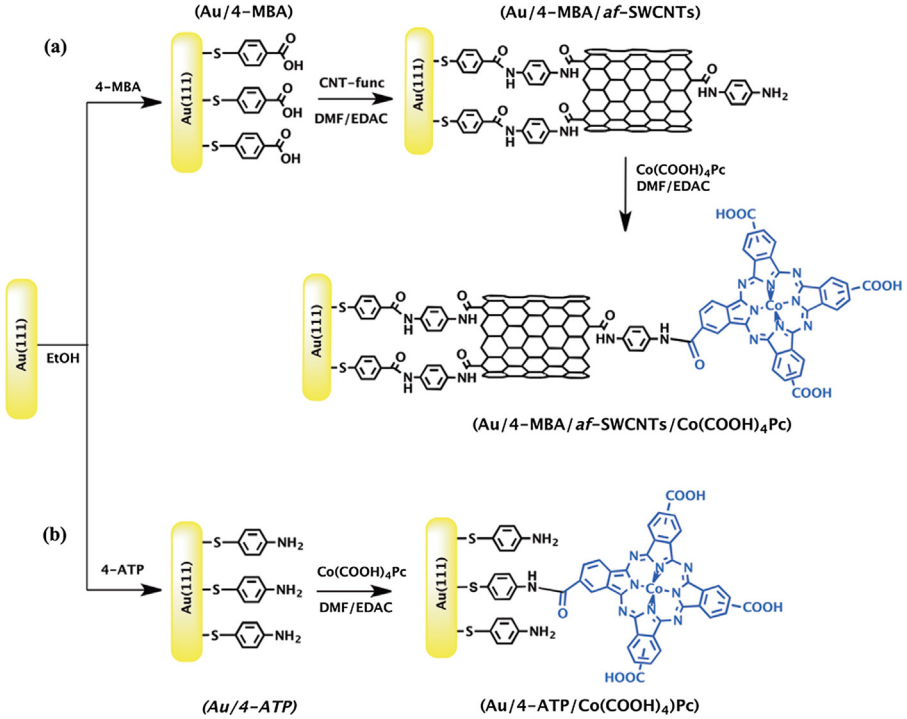


**Scheme 1.** Fabrication stages of (a) *Au/4-MBA/af-SWCNT/Co(COO)$_4$Pc* and (b) *Au/4-ATP/Co(COO)$_4$Pc*, assembled electrodes.

the product, *ox*-SWCNTs, was characterized using infrared spectroscopy (FT-IR) (Fig SD1). See Supplementary Information section 2 for more details.

### 2.4. Preparation of self-assembled monolayers, SAMs

Gold substrates were immersed in an absolute ethanol solution containing 50 μM of aromatic thiols (4-ATP and 4-MBA) for 24 hours at ambient temperature. The electrodes were then washed with ethanol to remove weakly adsorbed molecules and were then dried in a stream of high-purity $N_2$. The SAMs were formed by chemisorption of sulfur head group of aromatic thiols on Au(111), these substrates are denoted as: Au/4-MBA and Au/4-ATP.

### 2.5. Fabrication of Au/4-MBA/af-SWCNT/Co(COOH)4Pc and Au/4-MBA/af-SWCNT/Co(COO)4Pc Assembled Electrodes

The construction of the assembled electrode was conducted through two main steps (Scheme 1, part a). The first step involved the anchoring and vertical alignment of amino-functionalized (*af*-SWCNT) carbon nanotubes on Au/4-MBA preformed SAMs; in the second one, the covalent binding $Co(COOH)_4Pc$ catalyst complex to the *af*-SWCNT is achieved. The assembly of *af*-SWCNTs on *Au/4-MBA* SAMs was reached by the activation of the carboxyl groups in the SAMs, which was achieved by a carbodiimide coupling agent (EDAC) according to reported methods [55,56]. The gold substrates pre-modified with SAMs of 4-MBA were immersed in a DMF suspension with *af*-SWCNT (0.2 mg/mL), EDAC (1.3 mM) and HOBt (1.3 mM). The coupling reaction was carried out for 12 hours under stirring in the absence of light. Then, the substrates were then washed in DMF and dried with $N_2$. The substrate was denoted as Au/4-MBA/*af*-SWCNT. Once the assembly was obtained it was covalently functionalized with the $Co(COOH)_4Pc$ complex via amide bond formation. A mixture of EDAC (4.8 μM) and HOBt (4.8 μM) in DMF were added dropwise to a solution of Co $(COOH)_4Pc$ (4.8 μM), under constant stirring for 3 hours. The Au/4-MBA/*af*-SWCNT substrate was immersed in the solution for 12 hours under stirring in the absence of light. Subsequently, the electrodes were washed with an excess of pure solvent to remove unlinked species and subsequently dried with $N_2$. This substrate is denoted as Au/4-MBA/*af*-SWCNT/$Co(COOH)_4Pc$.

The functionalization of the complex on Au/4-ATP was performed using the previous methodology: the premodified substrate with 4-ATP was immersed in the $Co(COOH)_4Pc$-activated solution (by EDAC and HOBt) for 12 hours under the same conditions, followed by washing and drying with $N_2$ (Scheme 1, part b). This substrate was denoted as Au/4-ATP/$Co(COOH)_4Pc$.

**Schematic 1.** Diagram for fabrication of (a) *Au/4-MBA/af-SWCNT/Co(COO)$_4$Pc* and (b) *Au/4-ATP/Co(COO)$_4$Pc,* assembled electrodes.

## 3. Theoretical calculations

Theoretical computations were performed to explore structural and electronic properties of the Au/4-MBA/*af*-SWCNT/$Co(COO)_4Pc$ and Au/4-ATF/$Co(COO)_4Pc$ systems. The CNTs/$Co(COOH)_4Pc$ systems were considered for the calculations, where the chemical interaction takes place through the amine functionalized CNT. Note that the Au/SAMs surface was omitted from calculations to avoid the high computational cost. Three different CNTs were considered for the calculations, where the dangling bonds at the edges were saturated with hydrogen atoms: (9,0) metallic, (8,0) semi-metallic, and (8,1) semi-metallic. With these CNTs, three systems were modeled (Fig. 9): SWCNTs(9,0)/$Co(COO)_4Pc$ (*S1*), SWCNTs(8,0)/$Co(COO)_4Pc$ (*S2*) and SWCNTs(8,1)/$Co(COO)_4Pc$ (*S3*); additionally the free $Co(COOH)_4Pc$ complex (*Sc1*) and the SAMs structure 4-ATP/Co(COOH)4Pc (*Sc2*) were also considered for comparison purposes. All the molecular structures were pre-optimized at the semiempirical PM6 [57] level of theory in MOPAC2012 program [58]. Subsequently, the most stable CNT/$Co(COOH)_4Pc$ models

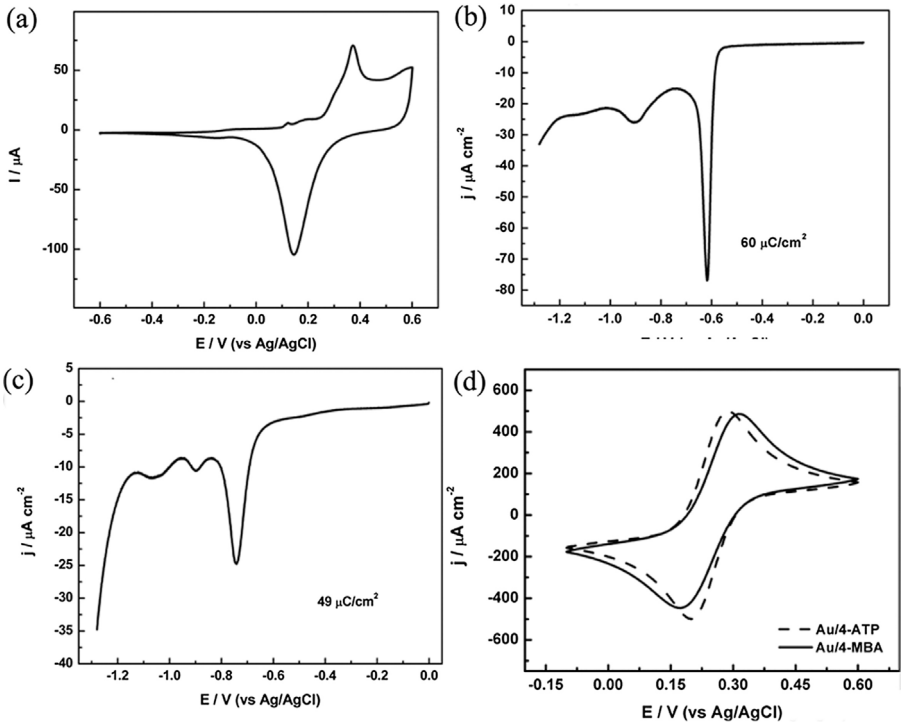


**Fig. 1.** Cyclic voltammograms for (a) unmodified Au(111) electrode, the reductive desorption of: (b) 4-MBA/SAMs, (c) 4-ATP/SAMs in 0.1 M NaOH solution and (d) comparative CV for SAMs of the 4-MBA and 4-ATP in solution containing 2.5 mM each in $Fe(CN)_6^{3-}$ and $Fe(CN)_6^{4-}$ and 0.50 M KCl.

(including their interactions with L-cys) were fully optimized at the density functional theory level in the ORCA 3.0 program [59]. The PBE [60] functional was used in combination with the 6-31G (d) basis sets [61,62]; the LANL2DZ [63] basis set and pseudopotential was used for the cobalt atom. Wavefunction analyses were performed in the Gabedit program [64].

Reactivity indexes [chemical potential ($\mu$) and molecular hardness ($\eta$)] were also computed to evaluate the reactivity before the formation of adduct (*electrode – L-cys*). $\mu$ [65] is the tendency of electrons to escape from an equilibrium system, where the electrons flow from regions with greater potential to regions of lower potential. Moreover, $\eta$ [66] relates to the resistance imposed by a system to deform its electronic density distribution, and indicates how reactive a molecular system is. $\mu$ and $\eta$ were obtained as: $\mu = (\partial E/\partial N)\nu \approx (\varepsilon_{LUMO} + \varepsilon_{HOMO})/2$ and, $\eta = (\partial^2 E/\partial N^2)\nu \approx (\varepsilon_{LUMO} - \varepsilon_{HOMO})/2$, where $E$ is the total energy, $N$ the total electron number, $\nu$ the external potential and $\varepsilon_{HOMO}$, $\varepsilon_{LUMO}$ correspond to the energy of the frontier molecular orbitals HOMO and LUMO, respectively. Interaction energies of the formed adducts were also obtained as: $E_{int} = E_{AB} - (E_A + E_B)$, where $E_{AB}$ corresponds to the energy of the adduct and, $E_A$ and $E_B$ to the energy of the fragments: molecular assembly (nanotube-complex) and L-cys, respectively. The more negative values of $E_{int}$, the more stable the formed adducts are.

## 4. Results and discussion

### 4.1. Characterization of SAMs 4-MBA and 4-ATP on Au(111)

In order to follow the formation of SAMs on the gold electrode, Fig. 1 shows the comparison of the voltammetry profile of the unmodified and SAMs modified gold surfaces, realized in a deaerated aqueous NaOH solution. Fig. 1a illustrates the cyclic voltammogram of a naked Au(111) electrode obtained after annealing the Au specimen. The *i* vs *E* profile shows the typical shape in alkaline electrolyte for an Au(111) electrode with atomically smooth (111) surfaces. Contrarily, Fig. 1b and c illustrate the voltammetric response for the reductive desorption or stripping process of SAMs of 4-MBA and 4-ATP from the Au(111) surface, respectively. The stripping of the SAMs from the surface electrode was conducted in 0.1 M NaOH at 0.05 V/s. The very sharp desorption wave observed for 4-MBA at ca. −0.6 V suggests that the SAMs formed by this particular molecule are rather homogeneous. Additionally, a more negative broad weak peak is observed at ca. −0.9 V, indicating the desorption of 4-MBA molecules from other surface domains or atomic steps [67]. In contrast, the reductive desorption voltammogram of 4-ATP (Fig. 1c) shows a rather broad and negatively shifted wave, in addition to two more negative peaks, indicating the desorption of three different forms of 4-ATP adsorbed on Au. The molecular structure of 4-MBA suggests that significant lateral intermolecular interactions ($\pi$-stacking) could be taking place between thioaromatic moities once the SAMs is formed, which ultimately strongly influences the stability and the desorption process of the SAMs. The electrical charge associated with the monolayer of 4-MBA (60 $\mu C\,cm^{-2}$) is larger than the charge related to 4-ATP (49 $\mu C\,cm^{-2}$). This difference in coverage and the rather multiple desorption peak can be attributed to the electron donor caracter of the 4-ATP molecules that should be assembled less close-packed on the Au(111) surface, giving rise to a more open monolayer and a lower coverage than 4-MBA and poorly defined film structure in agreement with literature [68].

To investigate the electron transfer process between the SAMs and a redox probe, The cyclic voltammetric behaviors of both functionalized electrodes in 1.0 mM $K_3[Fe(CN)_6]$ containing 0.1 M KCl were studied using a potential scan rate of 0.050 $Vs^{-1}$. On Fig. 1d, a pair of peak shaped redox processes of $[Fe(CN)_6]^{3-/4-}$ is observed for both Au/4-ATP (dash line) and Au/4-MBA (solid line) SAMs, with the peak-to-peak separation ($\Delta E_p$) about 0.089 and 0.140 V for Au/4-ATP y Au/4-MBA, respectively. Both, the electrochemical reversibility and the redox peak current of $[Fe(CN)_6]^{3-/4-}$□ declined slightly due to the lower electron transfer rate at the interface of Au/4-MBA and this can be attributed to the negative charge repulsion between the ionized $COO^-$ groups in 4-MBA and the $[Fe(CN)_6]^{3-/4-}$ [69].

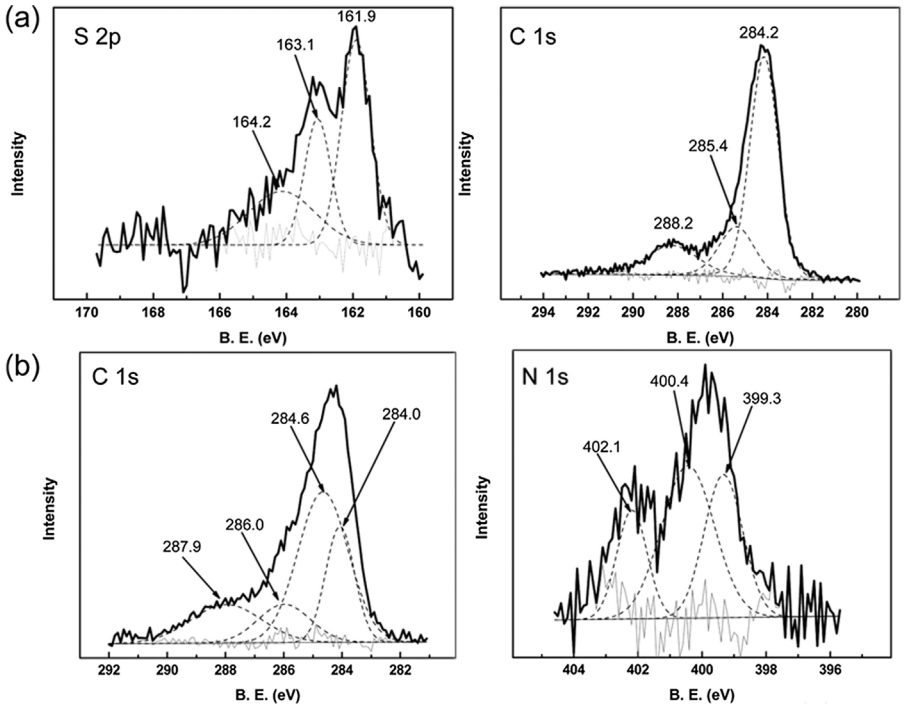


**Fig. 2.** X-ray photoelectron spectra for (a) Au/4-MBA of sulfur (S 2p) and carbon (C 1s) regions and for (b) Au/4-MBA/*af*-SWCNTs of carbon (C 1s) and nitrogen (N 1s) regions.

### 4.2. Characterization of Assembly of amine functionalized SWCNTs on pre-formed Au/4-MBA SAMs

The immobilization of the CNTs on the 4-MBA SAMs was performed via amide bond, between the terminal moieties of the self-assembled monolayer (-COOH) and the amino moieties of the CNT, according to step 2 of Scheme 1a. The modification of the electrode was confirmed using X-ray photoelectron spectroscopy (XPS). Fig. 2 shows the XPS spectra for the energy regions of most interests of the gold functionalized surface after the formation of the 4-MBA SAMs, and subsequent immobilization of *af*-SWCNTs onto this SAMs: sulphur, carbon for the Au/4-MBA (Fig. 2a) and carbon, nitrogen for the Au/4-MBA/*af*-CNT (Fig. 2b). The S (2p) spectrum consists of two peaks at 161.9 and 163.1 eV (assigned to the orbital doublet arising from S $2p_{3/2}$ and S $2p_{1/2}$) attributed to the Au-S bond and a peak at 164.2 eV that could indicate unbound (RSH) on the surface [70]. The 4-MBA SAMs showed three components for the C1 s at 284.2, 285.4 and 288.2 eV in agreement with literature for this SAMs [70]. The C (1s) spectrum for the *af*-CNT on the Au/4-MBA (Fig. 3b) appears a peak at 284.0 eV observed in the SAMs, a main peak centered on 284.6 eV is attributed to the C=C bond of the *af*-SWCNTs and two peak at 286.0 and 287.9 eV are associated to the amine (—N—C—) and amide (—N—C=O—) bonds, indicative of covalent bond formed between SAMs and carbon nanotube during self-assembly. Moreover, the N (1s) peaks observed at 399.3 and 400.3 eV assigned for the amine and amide groups, respectively, which confirms the attachment of the *af*-SWCNTs. Finally, the peak at ~402 eV was assigned to the R-$NH_3^+$ specie as observed by other authors [32].

Fig. 3a shows the electrochemical behavior of surfaces before and after the assembly of *af*-SWCNTs on the 4-MBA SAMs. The Au/4-MBA surface presents the typical voltammogram with redox peaks, whereas the Au/4-MBA/*af*-CNT surface voltammogram is characterized by a decline in the currents and the curve exhibits sigmoidal shape, characteristic behavior of systems in which diffusion fields do not overlap, and increase the mass transport rate [71–73] in a radial diffusion regime, in contrast to the typical transient form of massive electrodes found in the previous system, where the diffusion field is one-dimensional or linear. In this way, it is suggested that the Au/4-MBA/*af*-CNT interface presents a long-range nanostructured surface arrangement with the nanotubes vertically aligned to the substrate. On the other hand, the significant decrease in current of the system suggests that there are a smaller number of active sites with respect to the Au/4-MBA, because it is not possible to bond one nanotube to each molecule of 4-MBA SAMs. Therefore, it is suggested that the electro-active surface area of the Au/4-MBA/*af*-CNT system is smaller.

AFM images of Fig. 3b and c show that the carbon nanotubes immobilized on the 4-MBA SAMs provides a shape of needles-like or "saw tooth", typically of vertically aligned nanotubes due to differences in tube lengths (with average heights of ~94 nm), in agreement with previous reports [30,54,74]. On the other hand, the *af*-CNT can undergo interaction of the walls with the monolayer of the 4-MBA, resulting in a "mixed-array" arrangement with zones of nanotubes lying-down, as observed in the AFM image. This phenomenon is difficult to eliminate completely, since the immobilization of *af*-CNT is carried out without templates.

### 4.3. Characterization of the Au/4-ATP/Co(COOH)$_4$Pc and Au/4-MBA/af-SWCNT/Co(COOH)$_4$Pc Assembled Electrodes

The Co(COOH)$_4$Pc complex was attached to the pre-modified electrode (last step Scheme 1a y 1b) through at least one of the peripheral substituents (-COOH) of the complex. Cyclic voltammetry was used to obtain more insights into the assembled electrodes and their previous step of modification. Fig. 4a shows the voltammetric profiles of Au/4-ATP and Au/4-ATP/Co(COOH)$_4$Pc systems in pH 9.1 buffer solutions. The redox process, common for both surfaces, is attributed to the oxidation of 4-ATP generating a radical cation and a reversible redox coupled centered at ~0.10 V (black arrow) due to the formation of the pair benzoquinone/hydroquinone [75]. In addition, the Au/4-ATP/Co(COOH)$_4$Pc

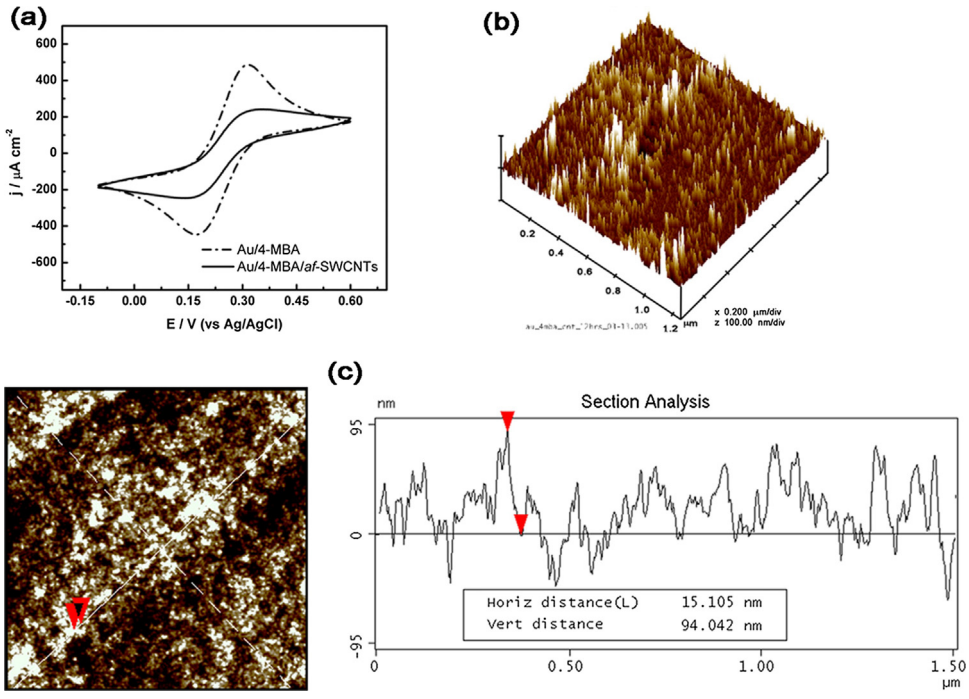


**Fig. 3.** (a) Comparative cyclic voltammograms for systems Au/4-MBA and Au/4-MBA/*af*-SWCNTs, in a solution containing 2.5 mM each in $Fe(CN)_6^{3-}$ and $Fe(CN)_6^{4-}$ and 0.50 M KCl. Atomic Force Microscopy (Tapping mode) analysis of the modified electrode Au/4-MBA/*af*-SWCNTs images: (b) a 3D view of surface and, (c) 2D image and the corresponding cross section analysis.

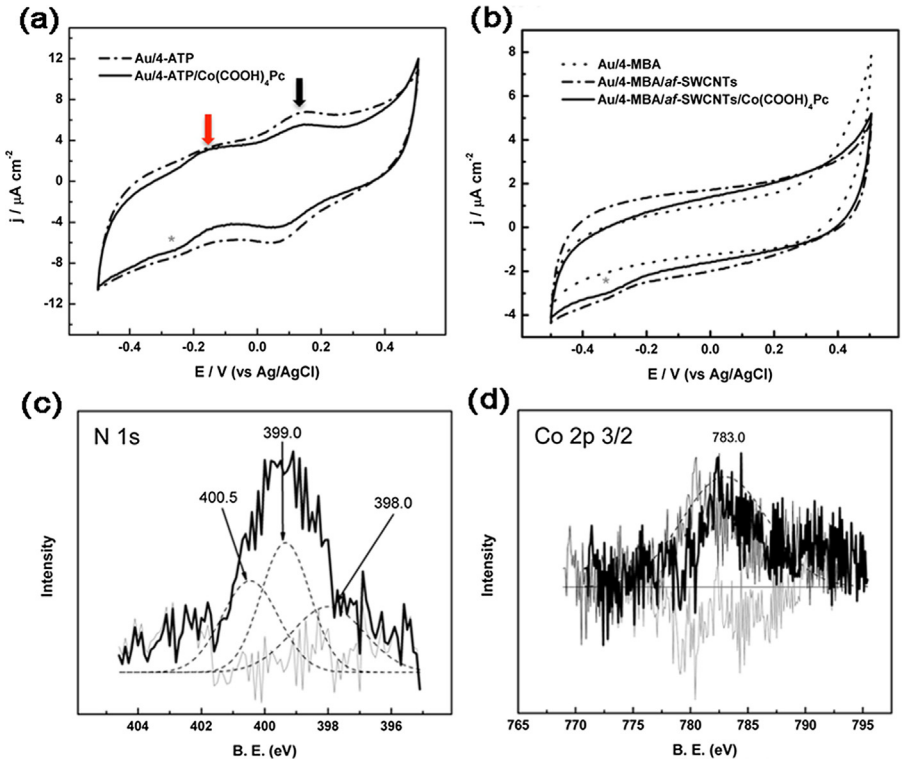


**Fig. 4.** (a) and (b) Comparison of cyclic voltammograms of all modified electrodes, performed in phosphate buffer solution pH. X-ray photoelectron spectra of (c) nitrogen (N 1s) and (d) cobalt (Co 2p $_{3/2}$) regions for Au/4-MBA/*af*-SWCNTs/$Co(COOH)_4Pc$.

electrode shows a signal at around −0.15 V (red arrow), possibly due to the Co(I)→Co(II) transition process of the complex; besides, a cathodic peak (*) at ∼0.25 V is observed corresponding to the reverse process, i.e. Co(II) →Co(I).

The surface coverage of the attachment complex was estimated from the plot of peak current ($i_p$) versus scan rate ($\nu$) using Eq. [76]:

$$i_p = \frac{\left(n^2F^2\nu A\Gamma\right)}{4RT}$$

where $i_p$ is the peak current (c.a. −0.15 V), $n$ the number of electrons transferred and equal to one? $F$ the Faraday's constant in Coulombs/equivalent, $\nu$ the scan rate in V/s, $A$ the electrode area, $\Gamma$ the surface coverage in mol/cm$^2$, $R$ the gas constant and $T$ is temperature in $K$. The $\Gamma$ was calculated to be $\approx 1 \times 10^{-12}$ mol/cm$^2$, which is close to a monolayer, depending on the diameter perpendicular to the surface occupied by each 4-ATP/Co(COOH)Pc ensemble. Therefore it is suggested that the 4-ATP SAMs could not be completely covered by the phthalocyanines complex.

Fig. 4b compares the cyclic voltammograms of Au/4-MBA, Au/4-MBA/*af*-SWCNT and Au/4-MBA/*af*-SWCNT/$Co(COOH)_4Pc$, in pH 9.1 buffer solutions, which does not present defined redox processes. The modification of 4-MBA SAMs with *af*-SWCNT results in an

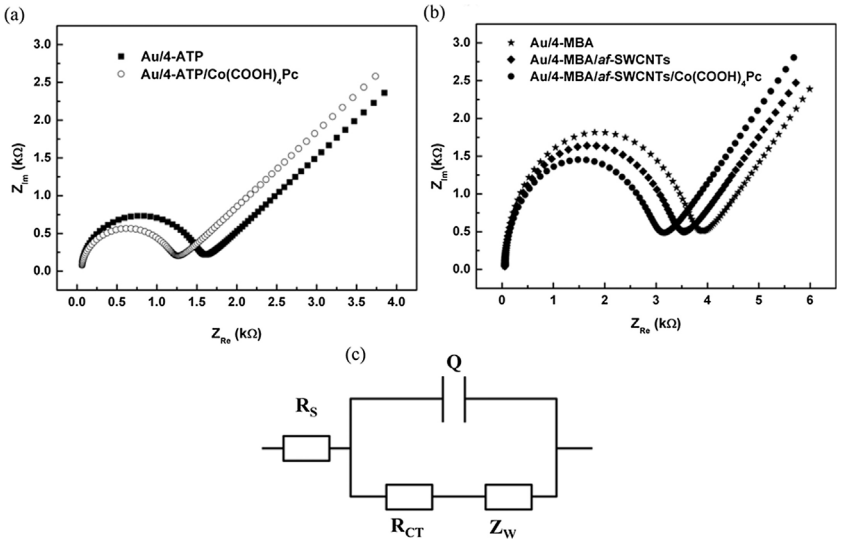


**Fig. 5.** Nyquist plot of the assembled systems (a) Au/4-ATP/$Co(COOH)_4Pc$ and (b) Au/4-MBA/*af*-SWCNTs/$Co(COOH)_4Pc$ systems, in 0.1 M KCl solution in the presence of 2.5 mM $[Fe(CN)_6]^{3-/4-}$; and (c) Randles model proposed.

increase of the capacitive current due to the incorporation of CNTs to the electrode surface. In the Au/4-MBA/*af*-SWCNT/Co(COOH)$_4$Pc assembled electrode, it is not possible to observe metal-centered redox processes most likely due to a more heterogeneous interface. A weak cathodic peak (*) is observed at ~ −0.31 V present only in this last electrode which can be attributed to the Co(II) →Co(I) process in the immobilized phthalocyanine, thus confirming its presence, such as for the Au/4-ATP/Co(COOH)$_4$Pc assembled electrode where this process is located at ~0.25 V. That is, the assembly of *af*-SWCNT to Au/SAMs would be causing a negative displacement of 60 mV in the redox potential of Co(II). The presence of the Co(COOH)$_4$Pc complex in the system was also evaluated using XPS experiments. Fig. 4c shows the Nitrogen (N 1s) region for the Au/4-MBA/af-SWCNT/Co(COOH)$_4$Pc electrode, where three contributions can be distinguished: a peak located at 398.0 eV attributed to phthalocyanine [77] and two other peaks at higher energy (400.5 and 399.3 eV) which were assigned to the amide and amine functional groups present in CNTs. These peaks differ slightly in energy because the XPS technique is very sensitive to the electronic environment of the atom. In addition, a weak peak was observed in the binding energy (BE) of ~ 783 eV (Fig. 4d) attributed to Co(II) (Co 2p$_{3/2}$) [77].

The results obtained, by the electrochemistry and XPS experiments, confirm the incorporation of the Co(COOH)$_4$Pc complex to the two assembled systems.

### 4.4. Electrochemical impedance spectroscopy

Electrochemical impedance spectroscopy is used to characterize the charge transfer process at the assembled electrodes. The Nyquist plot of the systems is presented in Fig. 5a and b. The measurements were performed in 0.1 M KCl in the presence of an outer- sphere redox probe $[Fe(CN)_6]^{3-}/^{4-}$. In both plots, it is possible to distinguish two regions: at high frequency, the kinetically controlled region, which is characterized by a half circle, where the diameter of this corresponds to the electron-transfer resistance ($R_{CT}$); a smaller diameter of the semicircle indicates a faster electronic transfer. At low frequency, we found the diffusion-controlled region, where the straight line or Warburg line is located.

The impedance spectra were fitted to the Randles' equivalent circuit shown in Fig. 7c. In the model, $R_S$ is the solution resistance, $R_{CT}$ corresponds the electron-transfer resistance, $Q$ represents the double layer capacitance and $Z_W$ is the Warburg impedance, which represents a kind of resistance to mass transfer [78]. Table 1 shows a summary of the estimated impedance parameters for the Randles' model. The $R_S$ and $Z_W$ elements values do not undergo significant changes after modification of the substrates, because they are not affected by the chemical transformations that occur at the interface (they represent bulk solution properties). Also, it is observed that the values obtained for $R_S$ are in agreement with similar electrodic systems under the same experimental conditions [75].

In both assembled systems, the highest $R_{CT}$ values were observed for Au/SAMs (4-ATP and 4-MBA), indicating that the monolayer has the lower conductivity and that imposes a barrier to the electronic transfer. The highest value of $R_{CT}$ is shown for Au/4-MBA, which could be due to the electrostatic repulsions produced at the interface between the deprotonated carboxyl groups of the 4-MBA monolayer (-COO$^-$) and the negatively charged redox probe $[Fe(CN)_6]^{3-}/^{4-}$ (at pH ~ 7). By introducing the *af*-SWCNT to the Au/4-MBA system, it is observed that the $R_{CT}$ decreases by 0.45 kΩ, which is expected due to the high electrical conductivity of the CNTs that facilitate electronic transport [79]. Some authors suggest that SWCNTs would allow electronic transfer via electron tunneling between the gold substrate and the redox probe present at the assembly/electrolyte interface, increasing the electron transfer [80]. The smaller $R_{CT}$ values were observed in the systems containing the complex, for Au/4-ATP/Co(COOH)$_4$Pc the resistance decreases approximately 0.3 kΩ with respect to the Au/4-ATP and for Au/4-MBA/*af*-SWCNT/Co(COOH)$_4$Pc the decrease in $R_{CT}$ is ~1.28 kΩ with respect to Au/4-MBA/*af*-SWCNT. The fact that the $R_{CT}$ value for the above mentioned systems is significantly smaller than the other electrodes could be due to the excellent electronic properties of phthalocyanine complex as well as due to attractive electrostatic interactions between the positively-charged metal center of the complex ($Co^{2+}$) with the negatively-charged redox probe $[Fe(CN)_6]^{3-}/^{4-}$. Finally, the electrochemical impedance data showed that the consecutive modification of the electrode results in molecular architectures that favor the electronic transport and yield high path for electron conduction between the electrochemical probe $[Fe(CN)_6]^{3-}/^{4-}$ and the electrode.

**Table 1**
Summary of estimated electrochemical impedance parameters obtained for all systems.

| Electrode | $R_S$ (kΩ) | $R_{CT}$ (kΩ) | $Z_W$ (mMho) |
|---|---|---|---|
| Au/4-ATP | 56.0 | 1.40 | 378 |
| Au/4-ATP/Co(COOH)$_4$Pc | 58.1 | 1.10 | 346 |
| Au/4-MBA | 50.3 | 3.56 | 375 |
| Au/4-MBA/*af*-SWCNTs | 55.6 | 3.21 | 322 |
| Au/4-MBA/*af*-SWCNTs/Co(COOH)$_4$Pc | 55.5 | 2.83 | 308 |

### 4.5. Electrocatalysis of L-cysteine oxidation

It is well known that the oxidation reaction of L-cys occurs at high potentials on conventional electrodes. Chemical modification of the surface has resulted in a remarkable improvement in the electrocatalytic response of the so modified electrode for the amino acid oxidation, using MN4 metal complexes such as metal porphyrins and metal phthalocyanines as electrocatalysts confined on graphite or carbon electrodes by simple adsorption [45], by deposition as thin films of complex polymers [46] or on gold electrodes functionalized with self-assembled monolayers of organo-thiolates capped with Co phthalocyanines [47]. In this regard, the electrocatalytic activity of our assembled electrodes was tested for the oxidation of L-cys, using cyclic voltammetry and slow potential scan linear voltammetry. Fig. 6a shows the cyclic voltammograms of all modified electrodes recorded in 1 mM L-cys in a phosphate buffer solution (pH = 9.1). No anodic peaks are observed on the Au/4-ATP, Au/4-MBA and Au/4-MBA/*af*-SWCNT surfaces, because SAMs and carbon nanotubes do not posses active sites for the oxidation of L-cys. However, the CV of L-cys on Au/4-ATP/Co(COOH)$_4$Pc and Au/4-MBA/*af*-SWCNT/Co(COOH)$_4$Pc show an irreversible anodic process at ~0.1 V that can be attributed to the oxidation of L-cys promoted by Co(COOH)$_4$Pc. Au/4-ATP/Co(COOH)$_4$Pc shows a well-resolved anodic peak with a onset potential at −0.19 V, value that is near the formal potential of the Co(II)/(I) redox process (Fig. 4a), indicating that the catalytic reaction is mediated by this redox couple. The voltammetric response of Au/4-MBA/*af*-SWCNT/Co(COOH)$_4$Pc shows a wider anodic peak and higher intensity than the previous system with a more negative onset potential (~ −0.38 V). The increase in the electrocatalytic activity of this system is evidenced by the displacement of the onset towards more negative potential values and by the significant increase in the current of the irreversible anodic peak of the oxidation of the L-cys. The catalytic process of the oxidation of L-cys involves in a first stage the formation of an adduct between the metal complex and the amino acid by means of metal-sulfur bonding [48]. In this process, the metal can change its oxidation state, resulting in its partial reduction. As we pointed above (section 4.3), in the Au/4-MBA/*af*-SWCNT/Co(COOH)$_4$Pc

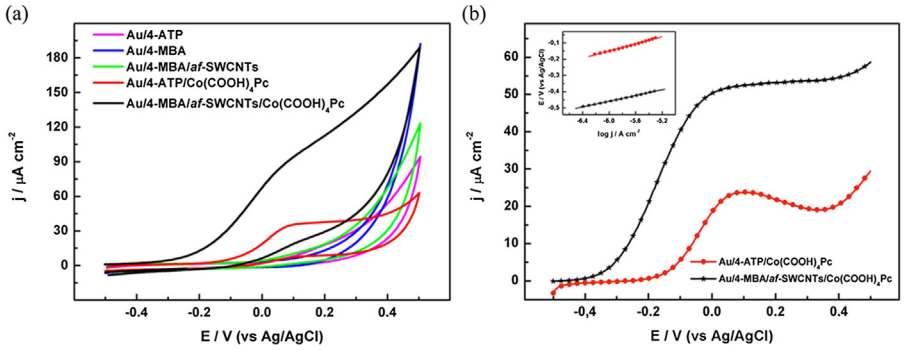


**Fig. 6.** (a) Comparison of the voltammetric response of all modified electrodes to 1 mM of L-cys oxidation, and (b) Polarization curves obtained from the oxidation of L-cysteine in phosphate buffer pH = 9.1. Insert: Tafel graph obtained from the polarization curves. Potential sweep speed: 2 $mVs^{-1}$.

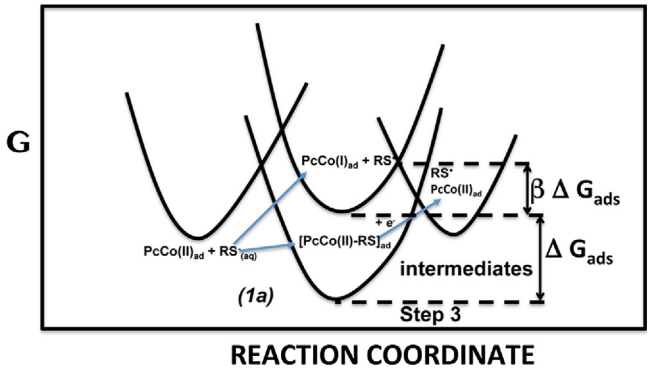


**Fig. 7.** Reaction coordinate profile for the oxidation reaction of L-cys.

ensemble, the potential of the Co(II)/(I) redox pair would experience a much greater negative displacement of its redox potential due to the incorporation of the CNTs between the SAMs and the $Co(COOH)_4Pc$ complex, of this way affecting their electrocatalytic activity [48,49]. The catalytic activity of CoN4 complexes for the oxidation of L-cys expressed as log (*i*)*E* versus the Co(II)/(I) redox potential varies in a non linear fashion [48]. Essentially it gives a volcano correlation. On one leg of the volcano the activity increases linearly with the Co(II)/(I) redox potential reaching a maximum and then it decreases also linearly. On the ascending leg and descending leg of the volcano several Co porphyrins and several Co phthalocyanines are located, respectively. So, for the case of the present work, a shift of the Co(II)/(I) redox potential in the negative direction compared to the complex adsorbed on the electrode surface will increase the catalytic activity. We could not detect the Co(II)/(I) transition at Au/4-MBA/*af*-SWCNT/$Co(COOH)_4Pc$ ensemble clearly enough as it is masked by the capacitive currents on the hybrid electrode, so we assume that the higher activity of $Co(COOH)_4Pc$ when located at the outmost location on the SAMs could attributed to a higher electron density on the Co center and this will move up the position of the catalyst in a hypothetical volcano correlation as that reported by our before [48]. Further in section 4.5 theoretical calculation shows that when SWCNTs are involved in the assembly the electron density on the Co center increases and this essentially agrees with what the volcano correlation predicts.

Kinetic studies were also performed in order to determine the Tafel slopes obtained from the corresponding Tafel plots and polarization curves (Fig. 6b), in a quasi-stationary regime. The Tafel linear relationship between *E* and log *j* is defined according to the following equation:

$$\boldsymbol{E = a + b}\ \log j$$

where *a* is the exchange current $i_0$ and *b* is the Tafel slope (with $b = 2.3\ RT/\alpha F$, for an oxidation process that is controlled by a first one-electron rate determining transfer step [50].

The Tafel slopes obtained were 110 and 90 mV/decade for Au/4-ATP/$Co(COOH)_4Pc$ and Au/4-MBA/*af*-SWCNT/$Co(COOH)_4Pc$, respectively. In the present case, a slope equal to 118 mV/decade (or $2.3 \times 2RT/F$) indicates that the first transfer of one electron to the thiol molecule is the rate determining step of the reaction, with an almost symmetrical energy barrier ($\alpha \sim 0.5$). In both systems the slopes are not far from 120 mV/decade, suggesting a common rate determining step is common for both configurations of Co $(COOH)_4Pc$ molecule. Thus, one could argue that the surface active site for L-cyst is the Co center and the molecular electronic structure of the Co-phthalocyanine is not changed very much when it is bound to ATP or bound to the SWCNT so the mechanism of the reaction should be the same.

A general mechanism for the oxidation of L-cys proposed in alkaline medium that agrees with th Tafel slope found is the following [51]:

$$RS^- + PcCo^{II} \leftrightarrows [PcCo^{I} - (SR)]^- \quad (1)$$

$$[PcCo^{I}\text{-}(SR)]^- \rightarrow [PcCo^{II} - (SR)] + e^- \qquad \text{rds} \quad (2)$$

$$[PcCo^{II}\text{-}(SR)] \rightarrow PcCo^{II} + RS^{\bullet} \quad (3)$$

$$RS^{\bullet} + RS^{\bullet} \rightarrow RS{-}RS^{\bullet} \quad (4)$$

where $RS^-$ corresponds to the deprotonated L-cys (p*K*a = 8.2) and $PcCo^{II}$ corresponds to the surface confined cobalt (II) phthalocyanine. It is known that in aqueous solution L-cyst reduced water soluble sulfonated Co(II) to Co(I) [42]. According to the mechanism, the key step is the binding of $Cys^-$ to the Co active site (step 1) with the simultaneous reduction of the metal center from Co(II) to Co(I). This process has been documented by spectroreflectance *in situ* studies of Co phthalocyanine adsorbed on the basal plane of graphite in the presence of L-cys. [42] The rate-determining step corresponds to step (2). However, this mechanism implies a chemical step 1 (bond forming) faster than electronic transfer, which is not in accordance with the theoretical results obtained (section 4.5), neither with the high electron transfer rate values observed for the catalytic process (Fig. 6b). Further, this mechanism has the drawback that if the formation of the $[PcCo^{I}\text{-}(SR)]^-$ species involves the stabilization of the $RS^-$ species, then the activation energy for the next step will be higher compared to a non-bound $RS^-$ species, i.e. no catalysis. Essentially,

$[PcCo^{I}\text{-}(SR)]^{-}$ will be in the bottom of an energy well. Step 1 involves bond formation and should be slow. So the mechanism presented above does not seem to explain the catalytic effect of the $Co(COOH)_4Pc$. The arguments given above also apply to step 3 that involves bond breaking as it implies important energy costs, The above mechanism would not account for the facility of the adduct rupture after the hypothetical slow electronic transfer in step 2. Therefore, the following three-step reaction mechanism agrees better with the experimental results:

$$RS^{-} + PcCo^{II} \leftrightarrows [PcCo^{II}\text{-}(SR)] + e- \quad \text{rds} \tag{1a}$$

$$[PcCo^{II}\text{-}(SR)] \rightarrow PcCo^{II} + RS^{\bullet} \tag{2a}$$

$$RS^{\bullet} + RS^{\bullet} \leftrightarrows RS\text{-}RS \tag{4}$$

In this mechanism, the slow step would correspond to (1a), where bond formation and oxidation of the L-cys occur simultaneously by transferring the one electron to the assembled electrode. The stabilization of the $[PcCo^{II}\text{-}(SR)]$ intermediate favors the reaction since it lowers the activation energy as illustrated in the scheme in Fig. 10. Additionally, the rupture of the adduct (2a) should faster than step (1a) which is now the rate determining step. Step (4) is well known to be very fast and thermodynamically favorable as thiol radicals are very unstable and highly reactive.

According to this mechanism, and neglecting the back reaction, the reaction rate is given by:

$$\boldsymbol{v = k_1\, \Gamma_{Co(II)}\, [L\text{-}cys](1-\theta)\, exp - [\alpha' \Delta G_{L\text{-}cys}/RT]\, exp + [\alpha EF/RT]}$$

where $k_1$ is the rate constant of step (1a), $\boldsymbol{\Gamma_{Co(II}}$ is the total surface concentration of active Co(II)Pc molecules in mol $cm^{-2}$, *[L-cys]* is the concentration of L-cys at the electrode surface in mol $cm^{-3}$, $\theta$ is the fraction of active sites covered by the thiolate or adduct $[PcCo^{II}\text{-}(RS)]$, $\Delta G_{L\text{-}cys}$ is the $\Delta G$ associated with the adsorption or coordination of the thiolate to the Co(II) active site, $E$ is the potential of the electrode vs. a reference electrode, $\alpha$' is a Brönsted factor that corresponds to the symmetry of the intersection of the energy parabolas in the transition state and $\alpha$ is the symmetry factor of the transition state corresponding to the charge transfer process which in this case coincides with $\alpha$' due the transition state is the same, i.e. the slow step (1a). We can suppose that the fraction of occupied sites $[PcCo^{II}\text{-}(RS)]$ is given by a Langmuir isotherm as the active sites are well separated from each other and then $\boldsymbol{\Delta G_{L\text{-}cys}}$ should be independent of coverage:

$$\theta = [\text{L-cys}]\, exp - \boldsymbol{[\Delta G_{L\text{-}cys}/RT]/[1 + [L\text{-}cys]\, exp - (\Delta L\text{-}cys/RT)]}$$

Which can be rewritten for $(1 - \theta)$:

$$\boldsymbol{(1-\theta) = 1/([L\text{-}cys]\, exp - [\Delta G_{L\text{-}cys}/RT])}$$

The role of the catalyst in the reaction is illustrated in Fig. 7 since as discussed before, the coordination of the thiolate to the Co (II) causes a decrease in the energy barrier, compared to the barrier where there is no Co-SR bond formation. This process then takes place in a concerted fashion with the electron transfer.

### 4.6. Analysis of the electronic structures

DFT calculations were performed for a better understanding of the previously described experimental data. Fig. 8a shows the

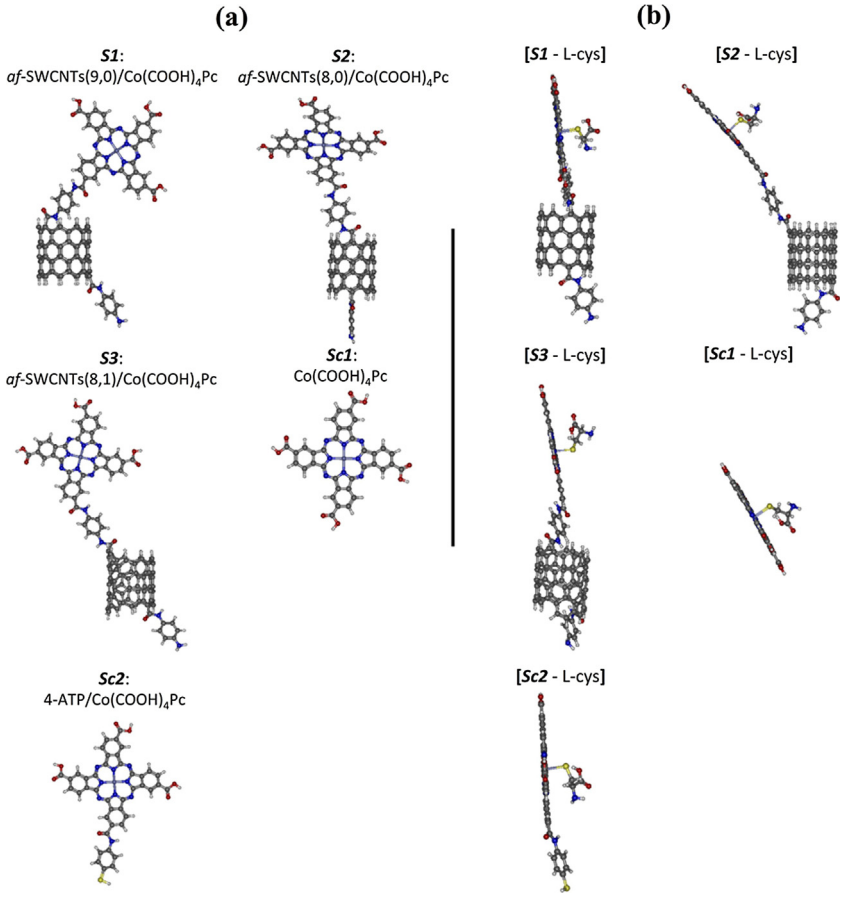


**Fig. 8.** (a) Molecular structures of the systems: S1- S3 and Sc and (b) molecular structures of the adduct formed between the systems: S1- S3 and Sc with l-cys, optimized at PBE/6-31G(d)/LANL2DZ level.

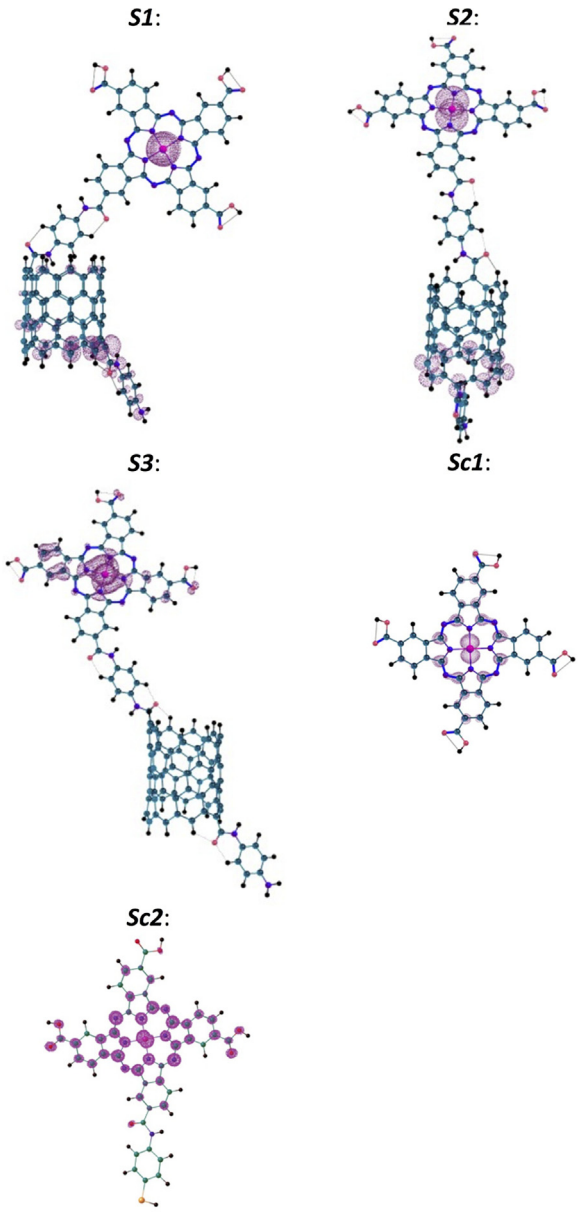


**Fig. 9.** LUMO molecular orbital of molecular arrangements: *S1*, *S2*, *S3* and *Sc*.

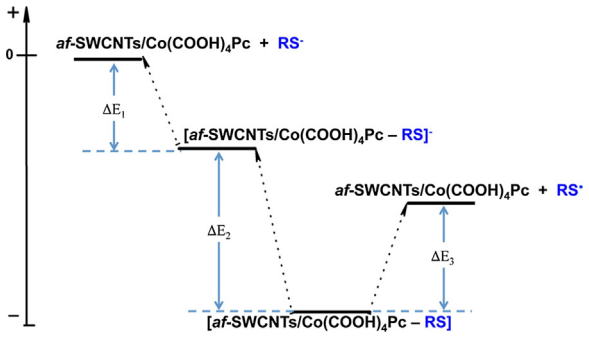


**Fig. 10.** Energy profile for all steps of the oxidation reaction of L-cys.

optimized structures of the five molecular arrangements: *S1*, *S2*, *S3*, *Sc1* and *Sc2*. These systems show a single attachment between the *af*-SWCNT with $Co(COOH)_4Pc$, which is an approximation because of the binding sites could be through more than one substituent of the complex. The optimized structures shows that the phthalocyanine is vertically placed when bound to *af*-SWCNT, this is inthe same vertical orientation as the nanotubes with a slight inclination of 18° in average, the same was observed for the phthalocyanine bound to 4-ATP (4-ATP/$Co(COOH)_4Pc$ system); then, both axial positions of the central metal remain available for the subsequent interaction with analytes (e.g. L-cys), unlike other systems reported in the literature [51].

On the other hand, the interaction of the *af*-SWCNTS/Co$(COOH)_4Pc$, free $Co(COOH)_4Pc$, and 4-ATP/$Co(COOH)_4Pc$ systems with L-cysteinate is displayed in Fig. 8b, which takes place by Co-S binding; note that L-cys is coordinated to the metal center when the oxidation reaction occurs. The Co-S bond distances (see the supporting information for details) of the *S1*, *S2* and *S3* systems are of the order of 2.45 Å, which are lower with respect to the free Co$(COOH)_4Pc$ complex and 4-ATP/$Co(COOH)_4Pc$ (~2.52 Å). The latter suggest an increase in the interaction strength, which is noted from the interaction energies ($\Delta E_{int}$) summarized in Table 3. For all the systems, the $\Delta E_{int}$ values are of the order of −49.40 to −52.34 kcal/mol, indicating that the formation of the five adducts are energetically favorable. However, the molecular systems containing the CNTs and 4-ATP showed that the adduct has greater stability, ~2 kcal/mol, with respect to the *Sc1* system. This suggests that both carbon nanotubes and 4-ATP SAM would affect the metallic center of the macrocycle displacing its Electronic cloud and this way the interaction between Co with L-cys would become more favorable in the first step of the oxidation mechanism compared to the free *Co(COOH)4Pc* complex. Note that for a single covalent bond is expected a bond order value close to 1.0; however, the dative Co-S bonding shows a bond order value of ~0.6. This result is expected for further steps, where the homolytic cleavage of the adduct must be reached without higher energies.

With respect to the electronic reactivity, Table 2 shows the $\mu$ and $\eta$ indexes of the molecular arrangements and their isolated fragments. Taking as starting point the free $Co(COOH)_4Pc$ complex, the data clearly show that as the system is assembled its electronic reactivity increases. Because of the low $\eta$ values are associated to the high electronic reactivity, it is observed the free *af*-SWCNT systems have the highest reactivity ($\eta \approx 0.03$ eV); while, the free Co$(COOH)_4Pc$ complex (corresponding to the *Sc1)* and 4-ATP/Co$(COOH)_4Pc$ (corresponding to the *Sc2)* showed the lowest reactivity with respect to the other systems ($\eta = 0.51$ and 0.44 eV, respectively). Consequently, when the *af*-SWCNT/$Co(COOH)_4Pc$ assembled systems are formed, an relatively high reactivity is reached, with $\eta$ values in the range of 0.07 to 0.14 eV. Furthermore, the $\mu$ index (which is associated to the negative of the Mulliken electronegativity [81]) shows that the free $Co(COOH)_4Pc$ complex has the highest electrophilic character among all the systems. Thus, when the complex is attached to the *af*-SWCNT, the electrophilic character of the assemblies is improved with respect to the isolated *af*-SWCNT. An analysis of the frontier molecular

**Table 2**
Reactivity descriptors molecular hardness ($\eta$) and chemical potential ($\mu$) of molecular and isolated systems obtained at PBE/6-31G(d)/LANL2DZ level, values in eV.

| Systems | Molecular Hardness | Chemical Potential |
|---|---|---|
| *S1* | 0.07 | -4.08 |
| *S2* | 0.14 | -4.10 |
| *S3* | 0.11 | -4.03 |
| *Sc1* | 0.51 | -4.62 |
| *Sc2* | 0.44 | -4.56 |
| *af*-SWCNTs(9,0) | 0.02 | -3.63 |
| *af*-SWCNTs(8,0) | 0.03 | -3.70 |
| *af*-SWCNTs(8,1) | 0.05 | -3.61 |
| L-cys ($RS^-$) | 1.80 | 1.90 |

**Table 3**
Energy difference of the steps involved in the L-cys oxidation reaction with systems *S1*-*S3* as shown in Fig. 10, and compared to control systems *Sc1* and *Sc2*. Energies are in kcal/mol.

| Systems | $\Delta E_1$ ($E_{int}$) | $\Delta E_2$ | $\Delta E_3$ | $\Delta E_{TOTAL}$ |
|---|---|---|---|---|
| *S1* | -52.34 | -84.70 | 33.49 | -103.55 |
| *S2* | -51.92 | -83.31 | 34.46 | -100.77 |
| *S3* | -51.34 | -81.98 | 35.49 | -97.83 |
| *Sc1* | -49.40 | -74.34 | 40.90 | -82.84 |
| *Sc2* | -51.60 | -72.65 | 44.80 | -79.45 |

orbitals (Fig. 9) (see the supporting information for details) shows that the LUMO (lowest unoccupied molecular orbital) has an important contribution in the metal center of the *af*-SWCNT/Co(COOH)$_4$Pc systems; thus the electrophilic character is still retained in the metal center, which is expected to acts as the active site for the nucleophilic attack of the L-cys, favoring the oxidation of this thiol. In addition, it is worth noting that the μ values of all the systems (*S1*, *S2*, *S3*, *Sc1* and *Sc2*) are lower with respect to the deprotonated L-cys ($RS^-$); then, the electrons should flow from the amino acid to the assemblies, suggesting the good setting for the oxidation reaction. Therefore, the covalent interaction of the CNTs with the Co(COOH)$_4$Pc complex has the expected synergistic effect, improving the properties presented by each component and provides a favorable scenario for the electrochemical reaction.

### 4.7. Interaction Energies

In order to obtain more information regarding each stage of the L-cys oxidation reaction with the *S1*, *S2*, *S3*, *Sc1 and Sc2* systems, Fig. 10 shows the energy profile where the relative energy of the involved processes is displayed: formation of the adduct, oxidation of the amino acid, and the homolytic cleavage of the adduct. The energy difference between the adduct and the free fragments is denoted as $\Delta E_1$, also called the interaction energy ($E_{int}$):

$$\Delta E_1 = E_{[af\text{-}SWCNT/Co(COOH)4Pc\text{-}RS]^-} - (E_{af\text{-}SWCNT/Co(COOH)4Pc} + E_{RS^-}) \quad (1)$$

Additionally, the $\Delta E_2$ and $\Delta E_3$ values correspond to the energies involved in the amino acid oxidation and in the rupture of the oxidized adduct, respectively:

$$\Delta E_2 = E_{[af\text{-}SWCNT/Co(COOH)4Pc\,-\,RS]} - E_{[af\text{-}SWCNT/Co(COOH)4Pc\,-\,RS]^-} \quad (2)$$

$$\Delta E_3 = (E_{[af\text{-}SWCNT/Co(COOH)4Pc} + E_{RS^\bullet}) - E_{[af\text{-}SWCNT/Co(COOH)4Pc\,-\,RS]} \quad (3)$$

Table 3 shows the $\Delta E_1$, $\Delta E_2$ and $\Delta E_3$ values for the four molecular systems. The $\Delta E_1$ values indicate that the formation of all adducts are energetically favorable as noted above, especially those systems with CNTs and 4-ATP SAM (*S1* > *S2* > *Sc2* > *S3*). The next step corresponding to the oxidation of L-cys ($\Delta E_2$) corresponds to an exergonic process; therefore, the system does not require additional energy to oxidize the L-cys. It was observed that in the *S1*, *S2* and *S3* systems, the process is even more favorable with respect to *Sc1* and *Sc2* in ~7.6 and ~9.3 kcal/mol, respectively; this result is in agreement with the experimental trend, where the oxidation reaction requires less energy (a more negative onset potential) in comparison with the usage of the *af*-SWCNT systems. In the last step, it is necessary to overcome a small energy barrier (positive $\Delta E_3$ values) of the order of ~38 kcal/mol; however, the interaction between 4-ATP and Co(COOH)$_4$Pc (Sc2) complex significantly increased the energy barrier ($\Delta E_3$ = 44.80 kcal/mol) of dissociate the adduct after oxidation. Finally, it can be observed that the overall reaction is an energetically favorable process, where the lower values of $\Delta E_{TOTAL}$ are obtained for the *S1*, *S2* and *S3* systems with values from −103.5 to −97.83 kcal/mol. The latter indicates the key role of the carbon nanotubes in the assemblies, which significantly favors the different steps of the catalytic reaction.

## 5. Conclusions

We have shown the construction of two electrodic assembled systems: Au/4-ATP/Co(COOH)$_4$Pc and Au/4-MBA/*af*-SWCNT/Co(COOH)$_4$Pc. Both systems proved to be good catalysts for the reaction of electro-oxidation of L-cys. Nevertheless, the system with *af*-SWCNTs showed an improved catalytic activity with respect to Au/4-ATP/CoPc(COOH)$_4$: more negative oxidation potentials and higher anodic peak currents. The analysis of the Tafel slope (≥120 mV/decade) suggests for both systems that the rate determinant step is the transfer of the first and only electron. The large surface array of functionalized SWCNTs provide an easy pathway for fast electron transfer, and increases the electrophilic character of the metal center of Co(COOH)$_4$Pc complex by promoting the nucleophilic attack of the L-cys favoring the oxidation of this thiol.

The electrochemical impedance spectroscopy showed that incorporation of *af*-SWCNTs and Co(COOH)$_4$Pc decreased the energy barrier to the charge transfer imposed by the monolayers on Au(111). Theoretical calculations performed by density functional theory showed a good correlation with the experimental results obtained in the analysis of: geometrical parameters, reactivity descriptors and interaction energy, among others; validating the models used and the calculation methodology. Further, it is suggested that the *af*-SWCNTs increased the reactivity of the assembly to the electronic transfer and in energy terms, the electrooxidation reaction is favorable.

## Acknowledgement

FONDECYT-Chile Grants 1171449, 1140199, 1140192 and Proyecto Basal USA 1555-VRIDEI PUBLIC 021742PI Universidad de Santiago de Chile supported this work.

M.S-N and J.E-V. are thankful to Conicyt for Doctoral fellowships. J.Z. is grateful to Dicyt-USACH. I.D.-P. thanks the Spanish MINECO CTQ2015-64579-C3-3-P for financial support. Powered@NLHPC: This research was partially supported by the supercomputing infraestructure of the NLHPC (ECM-02).

## Appendix A. Supplementary data

Supplementary data associated with this article can be found, in the online version, at http://dx.doi.org/10.1016/j.electacta.2017.09.082.

## References

[1] D.M. Guldi, G.M.A. Rahman, M. Prato, N. Jux, S. Qin, W. Ford, Single-Wall Carbon Nanotubes as Integrative Building Blocks for Solar-Energy Conversion, Angew. Chem. Int. Ed. 117 (2005) 2051–2054.
[2] P.J.F. Harris, Carbon Nanotubes and Related Structures, 1st edition, Cambridge University Press, Cambridge, 1999.
[3] F. Langa, M.J. Gómez-Escalonilla, P. Cruz, Carbon nanotubes and porphyrins: an exciting combination for optoelectronic devices, J. Porphyr. Phthalocya. 11 (2007) 348–358.
[4] X. Guo, L. Huang, S. O'Brien, P. Kim, C. Nuckolls, Directing and Sensing Changes in Molecular Conformation on Individual Carbon Nanotube Field Effect Transistors, J. Am. Chem. Soc. 127 (2005) 15045–15047.
[5] J. Wang, Carbon-Nanotube Based Electrochemical Biosensors: A Review, Electroanalysis 17 (2005) 7–14.
[6] J. Li, J.E. Koehne, A.M. Cassell, H. Chen, H.T. Ng, Q. Ye, W. Fan, J. Han, M. Meyyappan, Inlaid Multi-Walled Carbon Nanotube Nanoelectrode Arrays for Electroanalysis, Electroanalysis 17 (2005) 15–27.
[7] J.H. Zagal, S. Griveau, K.I. Ozoemena, T. Nyokong, F. Bedioui, Carbon Nanotubes, Phthalocyanines and Porphyrins Attractive Hybrid Materials for

Electrocatalysis and Electroanalysis, J. Nanosci. Nanotechnol. 9 (2009) 2201–2214.
[8] J.H. Zagal, S. Griveau, M. Santander-Nelli, S.G. Granados, F. Bedioui, Carbon nanotubes and metalloporphyrins and metallophthalocyanines-based materials for electroanalysis, J. Porphyr. Phthalocya. 16 (2012) 713–740.
[9] K. Lee, J. Zhang, H. Wang, D.P. Wilkinson, Progress in the synthesis of carbon nanotube- and nanofiber-supported Pt electrocatalysts for PEM fuel cell catalysis, J. Appl. Electrochem. 36 (2006) 507–522.
[10] X. Sun, R. Li, D. Villers, J.P. Dodelet, S. Désilets, Composite electrodes made of Pt nanoparticles deposited on carbon nanotubes grown on fuel cell backings, Chem. Phys. Lett. 379 (2003) 99–104.
[11] C.-L. Sun, L.-C. Chen, M.-C. Su, L.-S. Hong, O. Chyan, C.-Y. Hsu, K.-H. Chen, T.-F. Chang, L. Chang, Ultrafine Platinum Nanoparticles Uniformly Dispersed on Arrayed CNx Nanotubes with High Electrochemical Activity, Chem. Mater. 17 (2005) 3749–3753.
[12] E. Fakiolu, A review of hydrogen storage systems based on boron and its compounds, Int. J. Hydrogen Energy 29 (2004) 1371–1376.
[13] J. Masa, K. Ozoemena, W. Schuhmann, J.H. Zagal, Electrocatalysis in Fuel Cells: A Non- and Low- Platinum Approach, Springer, New York, 2013.
[14] J. Masa, K. Ozoemena, W. Schuhmann, J.H. Zagal, Oxygen reduction reaction using N4-metallomacrocyclic catalysts: fundamentals on rational catalyst design, J. Porphyr. Phthalocya. 16 (2012) 761–784.
[15] A. Merkoçi, Carbon Nanotubes in Analytical Sciences, Microchim. Acta 152 (2005) 157–174.
[16] J. Wang, M. Musameh, Electrochemical detection of trace insulin at carbon-nanotube-modified electrodes, Anal. Chim. Acta 511 (2004) 33–36.
[17] S. Daniel, T.P. Rao, K.S. Rao, S.U. Rani, G.R.K. Naidu, H.-Y. Lee, T. Kaewi, A review of DNA functionalized/grafted carbon nanotubes and their characterization, Sens. Actuators B Chem. 122 (2007) 672–682.
[18] B.S. Sherigara, W. Kutner, F. D'Souza, Electrocatalytic Properties and Sensor Applications of Fullerenes and Carbon Nanotubes, Electroanalysis 15 (2003) 753–772.
[19] A. Salimi, R. Hallaj, G.-R. Khayatian, Amperometric Detection of Morphine at Preheated Glassy Carbon Electrode Modified with Multiwall Carbon Nanotubes, Electroanalysis 17 (2005) 873–879.
[20] G. Lu, L. Jiang, F. Song, C. Liu, L. Jiang, Determination of Uric Acid and Norepinephrine by Chitosan-Multiwall Carbon Nanotube Modified Electrode, Electroanalysis 17 (2005) 901–905.
[21] J.L. Bahr, E.T. Mickelson, M.J. Bronikowski, R.E. Smalley, J.M. Tour, Dissolution of small diameter single-wall carbon nanotubes in organic solvents? Chem Commun. 19 (2001) 193–194.
[22] U.J. Kim, C.A. Furtado, X. Liu, G. Chen, P.C. Eklund, Raman and IR spectroscopy of chemically processed single-walled carbon nanotubes, J. Am. Chem. Soc. 127 (2005) 15437–15445.
[23] T. Ramanathan, F.T. Fisher, R.S. Ruoff, L.C. Brinson, Amino-Functionalized Carbon Nanotubes for Binding to Polymers and Biological Systems, Chem. Mater. 17 (2005) 1290–1295.
[24] W. Chidawanyika, T. Nyokong, Characterization of amine-functionalized single-walled carbon nanotube-low symmetry phthalocyanine conjugates, Carbon 48 (2010) 2831–2838.
[25] R. Cao, R. Thapa, H. Kim, X. Xu, M.G. Kim, Q. Li, N. Park, M. Liu, J. Cho, Promotion of oxygen reduction by a bio-inspired tethered iron phthalocyanine carbon nanotube-based catalyst, Nat. Commun. 4 (2013) 2076–2082.
[26] T. Ferri, D. Frasca, O.A. de Fuentes, R. Santucci, M. Frasconi, Spatially oriented and reversible surface assembly of single-walled carbon nanotubes: a strategy based on π-π interactions, Angew. Chem. Int. Ed. Engl. 50 (2011) 7074–7078.
[27] B. Wu, J. Zhang, Z. Wei, S. Cai, Z. Liu, Chemical Alignment of Oxidatively Shortened Single-Walled Carbon Nanotubes on Silver Surface, J. Phys. Chem. B 105 (2001) 5075–5078.
[28] A. Chou, P.K. Eggers, M.N. Paddon-Row, J.J. Gooding, Self-Assembled Carbon Nanotube Electrode Arrays: Effect of Length of the Linker between Nanotubes and Electrode, J. Phys. Chem. C 113 (2009) 3203–3211.
[29] G. Liu, S. Wang, J. Liu, D. Song, An electrochemical immunosensor based on chemical assembly of vertically aligned carbon nanotubes on carbon substrates for direct detection of the pesticide endosulfan in environmental water, Anal. Chem. 84 (2012) 3921–3928.
[30] K.E. Moore, B.S. Flavel, A.V. Ellis, J.G. Shapter, Comparison of double-walled with single-walled carbon nanotube electrodes by electrochemistry, Carbon 49 (2011) 2639–2647.
[31] J. Yu, J.G. Shapter, J.S. Quinton, M.R. Johnston, D.A. Beattie, Direct attachment of well-aligned single-walled carbon nanotube architectures to silicon (100) surfaces: a simple approach for device assembly, Phys. Chem. Chem. Phys. 9 (2007) 510–520.
[32] B.I. Rosario-Castro, E.J. Contés-de-Jesús, M. Lebrón-Colón, M.A. Meador, M.A. Scibioh, C.R. Cabrera, Single-wall carbon nanotube chemical attachment at platinum electrodes, Appl. Surf. Sci. 257 (2010) 340–353.
[33] J. Zagal, S. Ureta-Zañartu, Electro-oxidation of hydrazine catalyzed by sulfonated phthalocyanines adsorbed on a graphite electrode, J. Electrochem. Soc. 129 (1982) 2242–2247.
[34] C. Linares, D. Geraldo, M. Paez, J.H. Zagal, Non-linear correlations between formal potential and Hammett parameters of substituted iron phthalocyanines and catalytic activity for the electro-oxidation of hydrazine, J. Solid State Electrochem. 7 (2003) 626–631.
[35] C.A. Caro, F. Bedioui, M.A. Páez, G.I. Cárdenas-Jiron, J.H. Zagal, Experimental and theoretical study of the activity of substituted metallophthalocyanines for nitrite electro-oxidation, J. Electrochem. Soc. 151 (2004) E32–E39.
[36] C.A. Caro, J.H. Zagal, F. Bedioui, Electrocatalytic activity of substituted metallophthalocyanines adsorbed on vitreous carbon electrode for nitric oxide oxidation, J. Electrochem. Soc. 150 (2003) E95–E103.
[37] S.L. Vilazi, T. Nyokong, Voltammetric determination of nitric oxide on cobalt phthalocyanine modified microelectrodes, J. Electroanal. Chem. 512 (2001) 56–63.
[38] G.I. Cárdenas-Jirón, J.H. Zagal, Donor-acceptor intermolecular hardness on charge transfer reactions of substituted cobalt phthalocyanines, J. Electro Anal. Chem 497 (2001) 55–60.
[39] J.H. Zagal, M.J. Aguirre, M.A. Páez, O2 reduction kinetics on a graphite electrode modified with adsorbed vitamin B12, J. Electroanal. Chem. 437 (1997) 45–52.
[40] N. Sehlotho, T. Nyokong, Effect of ring substituents on electrocatalytic activity of manganese phthalocyanines towards the reduction of molecular oxygen, J. Electroanal. Chem. 595 (2006) 161–167.
[41] J. Masa, W. Schuhman, Systematic selection of metalloporphyrin-based catalysts for oxygen reduction by modulation of the donnor-acceptor intermolecular hardness, Chem. Eur. J. 19 (2013) 9644–9654.
[42] R.O. Lezna, S. Juanto, J.H. Zagal, Spectroelectrochemical studies of tetrasulfonated metallophthalocyanines adsorbed on the basal plane of graphite in the presence of cysteine, J. Electroanal. Chem. 452 (1998) 221–228.
[43] J.H. Zagal, C. Páez, Catalytic electrooxidation of 2-mercaptoethanol on a graphite electrode modified with metal-phthalocyanines, Electrochim. Acta 34 (1989) 243–247.
[44] M.J. Aguirre, M. Isaacs, F. Armijo, L. Basáez, J.H. Zagal, Effect of the substituents on the ligand of iron phthalocyanines adsorbed on graphite electrodes on their activity for the electrooxidation of 2-mercaptoethanol, Electroanalysis 14 (2002) 356–362.
[45] M. Sekota, T. Nyokong, Catalytic behavior of osmium(II), rhodium(II) and ruthenium(II) phthalocyanines towards the electrooxidation of cysteine on glassy carbon electrodes, Electroanalysis 9 (1999) 1257–1261.
[46] X. Qi, R.P. Baldwin, Selective oxidation of thiols to disulfides at polymeric cobalt phthalocyanine chemically modified electrodes, J. Electrochem. Soc. 143 (1996) 1283–1287.
[47] K. Ozoemena, P. Westbroek, T. Nyokong, Long-term stability towards cysteine detection using gold modified with a self-assembled monolayer of octabutylthiophthalocyaninatocobalt (II), Electrochem. Commun. 3 (2011) 529–534.
[48] F.J. Recio, C.A. Gutierrez, R. Venegas, C. Linares-Flores, C.A. Caro, J.H. Zagal, Optimization of the electrocatalytic activity of MN4-macrocyclics adsorbed on graphite electrodes for the electrochemical oxidation of L-cysteine by running the M (II)/(I) formal potencial of the catalyst: an overview, Electrochim. Acta 140 (2014) 482–488.
[49] J.H. Zagal, S. Griveau, J.F. Silva, T. Nyokong, F. Bedioui, Metallophthalocyanine-based molecular materials as catalysts for electrochemical reactions, Coord. Chem. Rev. 254 (2010) 2755–2791.
[50] N. Sehlotho, T. Nyokong, J.H. Zagal, F. Bedioui, Electrocatalysis of oxidation of 2-mercaptoethanol: l-cysteine and reduced glutathione by adsorbed and electrodeposited cobalt tetra phenoxypyrrole and tetra ethoxythiophene substituted phthalocanines, Electrochim. Acta 51 (2006) 5125–5130.
[51] F. Bedioui, S. Griveau, T. Nyokong, A.J. Appleby, C.A. Caro, M. Gulppi, G. Ochoa, J. H. Zagal, Tuning the redox properties of metalloporphyrin- and metallophthalocyanine-based molecular electrodes for the highest electrocatalytic activity in the oxidation of thiols, Phys. Chem. Chem. Phys. 9 (2007) 3383–3396.
[52] K.I. Ozoemena, T. Nyokong, Comparative electrochemistry and electrocatalytic activities of cobalt, iron and manganese phthalocyanine complexes axially co-ordinated to mercaptopyridine self-assembled monolayer at gold electrodes, Electrochim. Acta 51 (2006) 2669–2677.
[53] M.S. Ureta-Zanartu, A. Alarcón, C. Berrios, G.I. Cárdenas-Jirón, J. Zagal, C. Gutierrez, Electropreparation and characterization of polyNiTSPc films. An EQCM study, J. Electroanal. Chem. 580 (2005) 94–104.
[54] K.I. Ozoemena, D. Nkosi, J. Pillay, Influence of solution pH on the electron transport of the self-assembled nanoarrays of single-walled carbon nanotube-cobalt tetra-aminophthalocyanine on gold electrodes: Electrocatalytic detection of epinephrine, Electrochim. Acta 53 (2008) 2844–2851.
[55] Z. Liu, Z. Shen, T. Zhu, S. Hou, L. Ying, Organizing Single-Walled Carbon Nanotubes on Gold Using a Wet Chemical Self-Assembling Technique, Langmuir 16 (2000) 3569–3573.
[56] X. Nan, Z. Gu, Z. Liu, Immobilizing shortened single-walled carbon nanotubes (SWNTs) on gold using a surface condensation method, J. Colloid Interface Sci. 245 (2002) 311–318.
[57] J.J.P. Stewart, Optimization of parameters for semiempirical methods V: modification of NDDO approximations and application to 70 elements, J. Mol. Model. 13 (2007) 1173–1213.
[58] J.J.P. Stewart, MOPAC, Stewart Computational Chemistry, Colorado Springs, CO, USA, 2012. http://OpenMOPAC.net.
[59] F. Neese, The ORCA program system, Wiley Interdiscip. Rev. Comput. Mol. Sci. 2 (2012) 73–78.
[60] J.P. Perdew, K. Burke, M. Ernzerhof, Generalized Gradient Approximation Made Simple, Phys. Rev. Lett. 77 (1996) 3865–3868.
[61] G.A. Petersson, A. Bennett, T.G. Tensfeldt, M.A. Al-Laham, W.A. Shirley, J. Mantzaris, A complete basis set model chemistry. I. The total energies of closed-shell atoms and hydrides of the first-row atoms, J. Chem. Phys. 89 (1988) 2193–2218.

[62] G.A. Petersson, M.A. Al-Laham, A complete basis set model chemistry. II. Open-shell systems and the total energies of the first-row atoms, J. Chem. Phys. 94 (1991) 6081–6090.
[63] P.J. Hay, W.R. Wadt, Ab initio effective core potentials for molecular calculations. Potentials for K to Au including the outermost core orbitals, J. Chem. Phys. 82 (1985) 299–310.
[64] A.-R. Allouche, Gabedit-a graphical user interface for computational chemistry softwares, J. Comput. Chem. 32 (2011) 174–182.
[65] R.G. Parr, R.A. Donnelly, M. Levy, W.E. Palke, Electronegativity The density functional viewpoint, J. Chem. Phys. 68 (1978) 3801–3807.
[66] R.G. Parr, R.G. Pearson, Absolute hardness: companion parameter to absolute electronegativity, J. Am. Chem. Soc. 105 (1983) 7512–7516.
[67] K. Arihara, T. Ariga, N. Takashima, K. Arihara, T. Okajima, F. Kitamura, K. Tokuda, T. Ohsaka, Multiple voltammetric waves for reductive desorption of cysteine and 4-mercaptobenzoic acid monolayers self-assembled on gold substrates, Phys. Chem. Chem. Phys. 5 (2003) 3758–3761.
[68] K.W. Hipps, X. Lung, X.D. Wang, U. Manzur, Metal d-orbital occupation-dependent images in the scanning tunneling microscopy of metal phthalocyanines, J Phys. Chem. B 100 (1996) 11207–11210.
[69] K.I. Ozoemena, T. Nyokong, D. Nkosi, I. Chambrier, M.J. Cook, Insights into the surface and redox properties of single-walled carbon nanotube—cobalt(II) tetra-aminophthalocyanine, Electrochim. Acta 52 (2007) 4132–4143.
[70] D. Barriet, C.M. Yam, O.E. Shmakova, A.C. Jamison, T.R. Lee, 4-Mercaptophenylboronic Acid SAMs on Gold: Comparison with SAMs Derived from Thiophenol, 4-Mercaptophenol, and 4-Mercaptobenzoic Acid, Langmuir 23 (2007) 8866–8875.
[71] K. Hirota, K. Tajima, K. Hashimoto, Facile Preparation of Nanoelectrode Ensembles Using Amphiphilic Block Copolymer Film, Langmuir 21 (2005) 11592–11595.
[72] A. Valsesia, P. Lisboa, P. Colpo, F. Rossi, Fabrication of Polypyrrole-Based Nanoelectrode Arrays by Colloidal Lithography, Anal. Chem. 78 (2006) 7588–7591.
[73] D.W.M. Arrigan, Nanoelectrodes: nanoelectrode arrays and their applications, Analyst 129 (2004) 1157–1165.
[74] J.J. Gooding, R. Wibowo, J. Liu, W. Yang, D. Losic, S. Orbons, F.J. Mearns, J.G. Shapter, D.B. Hibbert, Protein Electrochemistry Using Aligned Carbon Nanotube Arrays, J. Am. Chem. Soc. 125 (2003) 9006–9007.
[75] S.H. Cho, D. Kim, S.M. Park, Electrochemistry of conductive polymers, Electrochim. Acta 53 (2008) 3820–3827.
[76] D. Martel, N. Sojic, A. Kuhn, A simple student experiment for teaching surface electrochemistry: adsorption of polyoxometalate on graphite electrodes, J. Chem. Educ. 79 (2002) 349.
[77] G.E. Muilenberg, Handbook of x-ray photoelectron spectroscopy, Eden, Prairie Minnesota, 1979.
[78] A. Bard, L.R. Faulkner, Electrochemical Methods Fundamentals an Applications, John Wiley & Sons Inc, New York, 2001.
[79] I.A. Akinbulu, T. Nyokong, Fabrication and characterization of single walled carbon nanotubes-iron phthalocyanine nano-composite: surface properties and electron transport dynamics of its self assembled monolayer film, New J. Chem. 34 (2010) 2875–2886.
[80] P. Diao, Z. Liu, Electrochemistry at chemically assembled single-wall carbon nanotube arrays, J. Phys. Chem. B 109 (2005) 20906–20913.
[81] R.S. Mulliken, A new electroaffinity scale; together with data on valence states and on valence ionization potentials and electron affinities, J. Chem. Phys. 2 (1934) 782–793.